Journal of Computational Neuroscience 12, 55–73, 2002

Summation of Spatiotemporal Input Patterns in Leaky Integrate-and-Fire Neurons: Application to Neurons in the Cochlear Nucleus Receiving Converging Auditory Nerve Fiber Input

LEVIN KUHLMANN
Department of Otolaryngology, The University of Melbourne, Royal Victorian Eye and Ear Hospital, 32 Gisborne Street, East Melbourne, VIC 3002, Australia; The Bionic Ear Institute, 384–388 Albert Street, East Melbourne, VIC 3002, Australia

ANTHONY N. BURKITT
The Bionic Ear Institute, 384–388 Albert Street, East Melbourne, VIC 3002, Australia
a.burkitt@medoto.unimelb.edu.au

ANTONIO PAOLINI
Department of Otolaryngology, The University of Melbourne, Royal Victorian Eye and Ear Hospital, 32 Gisborne Street, East Melbourne, VIC 3002, Australia

GRAEME M. CLARK
Department of Otolaryngology, The University of Melbourne, Royal Victorian Eye and Ear Hospital, 32 Gisborne Street, East Melbourne, VIC 3002, Australia; The Bionic Ear Institute, 384–388 Albert Street, East Melbourne, VIC 3002, Australia

Received June 5, 2001; Revised December 19, 2001; Accepted January 4, 2002

Action Editor: Shihab Shamma

Abstract. The response of leaky integrate-and-fire neurons is analyzed for periodic inputs whose phases vary with their spatial location. The model gives the relationship between the spatial summation distance and the degree of phase locking of the output spikes (i.e., locking to the periodic stochastic inputs, measured by the synchronization index). The synaptic inputs are modeled as an inhomogeneous Poisson process, and the analysis is carried out in the Gaussian approximation. The model has been applied to globular bushy cells of the cochlear nucleus, which receive converging inputs from auditory nerve fibers that originate at neighboring sites in the cochlea. The model elucidates the roles played by spatial summation and coincidence detection, showing how synchronization decreases with an increase in both frequency and spatial spread of inputs. It also shows under what conditions an enhancement of synchronization of the output relative to the input takes place.

Keywords: spatiotemporal summation, synchronization, auditory pathway, integrate-and-fire neuron, temporal coding

1. Introduction

Information in the nervous system is carried by the action potentials (or spikes) that are generated by and transmitted between neurons. Both the timing of the action potentials (APs) (i.e., temporal information) and the identity of the spiking neuron (i.e., place information) convey aspects of the information contained in the neural code. There are a number of situations where the identity of the neuron is related to some external (e.g., spatial) dimension and where the spatial relationships between the neurons reflect this external structure, resulting in a *spatiotemporal* coding of information. Such interactions between spatial and temporal aspects of the neural code have been observed in a number of sensory systems, particularly the auditory system where the tonotopic organization of frequency has been extensively studied (von Békésy, 1960; Liberman, 1982; Webster et al., 1992), as well as in other more central parts of the nervous system, such as the hippocampus (Bose et al., 2000), cerebellum (Buonomano and Mauk, 1994), and visual cortex (receiving LGN inputs during stimulation by drifting gratings) (Hubel and Wiesel, 1962).

Spatiotemporal coding in the auditory system is generated within the cochlea, where the vibration of the basilar membrane (BM) gives rise to both a spatial and temporal representation of the frequency spectrum of the stimulus. The spatial (or tonotopic) organization is brought about by the frequency filtering properties of the BM, whereby the place at which maximum displacement occurs (the *characteristic place*, CP) varies from the base to the apex of the cochlea as the frequency of the stimulating tone varies from high to low (von Békésy, 1960). Auditory nerve (AN) fibers, which are stimulated by hair cells attached to the BM, display the tonotopic organization of their CP through their characteristic frequencies (CF) (the stimulus frequency at which an increase in spiking rate can be induced at the lowest stimulus intensity) determined by their responses to pure tones. Consequently the AN carries a *spatial* (or *spectral*) representation of the frequency (see Pickles, 1982, and Webster et al., 1992, for reviews).

In addition to this spectral information, the auditory pathway also carries *temporal* information. The peripheral auditory pathway has long been known as one of the major neural systems where temporal coding in neurons takes place (Galambos and Davis, 1943; Tasaki, 1954; Kiang et al., 1965; Rose et al., 1967; Lavine, 1971). Temporal coding in the peripheral auditory pathway has been observed in the form of phase locking to low frequency sinusoidal stimuli of up to 3 to 5 kHz in mammals (Rose et al., 1967; Lavine, 1971; Johnson, 1980; Joris et al., 1994a, 1994b). These phase locking neurons generate spikes at a preferred phase of the stimulus period and, as a result, respond with interspike intervals that are integer multiples of the stimulus period (Kiang et al., 1965; Rose et al., 1967; Lavine, 1971). The degree of phase locking of a neuron's response can be quantified by the synchronization index (SI), also known as the vector strength (Goldberg and Brown, 1969; Anderson, 1973; Johnson, 1980). The SI ranges between the value of one when the neuron response is locked tightly to a particular phase of the stimulus period and zero when the neuron responds equally at all phases of the stimulus period. Temporal coding has been shown to be important for sound localization (Rayleigh, 1876; Jeffress, 1948; Mills, 1958; Carr and Konishi, 1990; Gerstner et al., 1996), but its role in auditory tasks such as sound and speech recognition remains to be fully understood (see Greenberg, 1996, for a review).

The first stage of processing in the central auditory pathway is the cochlear nucleus (CN), whose neurons are the targets of the afferent AN fibers and whose temporal properties have been the subject of a number of studies (Eggermont et al., 1983; Carney, 1990, 1992; Carney and Friedman, 1998). Joris et al. (1994a, 1994b) examined the relationship between the output SI of antero-ventral cochlear nucleus (AVCN) neurons, which include bushy cells, and the SI of the incoming AN fibers. They demonstrated that the output SI of AVCN neurons relative to the SI of AN fibers from which they receive input was *enhanced* for stimulus frequencies up to approximately 0.7 kHz (and reduced at higher frequencies). A similar enhancement of synchronization at low frequencies has also been observed in the AVCN analogue in the barn owl (Köppl, 1997). Joris et al. (1994a, 1994b) showed that these results were consistent with those obtained by studying a single spiking-neuron model that employs coincidence detection (see Joris et al., 1998, and Kempter et al., 1998, for reviews of coincidence detection). They demonstrated that the degree of synchronization enhancement is dependent on various neural parameters such as the membrane potential decay time constant and the size of the input excitatory postsynaptic potential (EPSP) amplitudes relative to the spiking-threshold. An enhancement of synchronization requires the convergence of

two or more inputs onto the neuron and the coincidence of input spikes (i.e., a short temporal window of integration). More detailed studies of bushy cells using a single compartment model were able to identify a number of different response patterns corresponding to various ranges of the neural parameters (Rothman et al., 1993; Rothman and Young, 1996).

An important feature missing from both these studies was the question of how the output synchronization is affected by differences in the phases of arrival of AN fiber inputs that arise from their spatial distribution on the BM. One model that does address this question is that by Bruce et al. (1998), in which they analyze a mathematical model of spatiotemporal summation of AN firings based on the idea of input phase differences resulting from consecutive activation of AN fibers by the traveling wave of the BM (Ruggero and Rich, 1987). Their model uses a stochastic point process representation of AN fiber activity, where each fiber's response to a pure tone sound stimulus is described by the time-dependent mean and variance of its spiking-rate—i.e., a periodic/inhomogeneous Poisson process (Papoulis, 1991). A summing neuron (nonthresholded) was created, in which the output spiking-rate function was the sum of the spiking-rate functions for each input fiber. This summation was performed spatially, across an arbitrary number of (consecutively activated) AN fibers originating from a spread over the BM, and then temporally, over a fixed duration time window. This results in an output spiking-rate function that is the total of the input spiking-rate functions of the population of fibers considered, from which a measure of the synchronization of the population response can be obtained, termed the population SI (PSI). Their results demonstrated that the PSI is greatest for a narrow spread of AN fibers and drops off with both increasing frequency and summation distance. Due to the constraints of their summing neuron, Bruce et al. (1998) were unable to show an enhancement of synchronization or to address the question of whether thresholding neurons (i.e., neurons that generate an AP when their membrane potential reaches threshold) would be able to generate an enhancement of synchronization for narrow spreads of input along the BM. A number of studies have shown the importance of the threshold in the distribution of output spikes generated by coherent synaptic input (Maršálek et al., 1997; Burkitt and Clark, 1999; Salinas and Sejnowski, 2000).

The aim of this study is to better understand the spatiotemporal code, the way in which it is processed and transmitted, and the conditions under which an enhancement of synchronization can occur. In order to do this we use a thresholding neuron—namely, the leaky integrate-and-fire (LIF) neuron in which the membrane potential decays towards its resting value with a characteristic time constant, τ. The membrane potential is augmented by input spikes from individual afferent fibers that arrive at synapses on the soma and generate postsynaptic potentials (PSPs) that summate. The neuron generates an output spike when the membrane potential exceeds the firing threshold. The LIF neuron is one of the most widely used models for studying systems of neurons (see Tuckwell, 1988, for a review) and has been used extensively to study aspects of the auditory pathway (Molnar and Pfeiffer, 1968; Tuckwell and Richter, 1978; Colburn et al., 1990; Carney, 1992; Young et al., 1993; Joris et al., 1994a; Kalluri, 2000). The present study uses a recently developed technique for analyzing the LIF neuron (Burkitt and Clark, 1999, 2000, 2001; Hohn and Burkitt, 2001) that allows the calculation of the output SI given that the inputs to the model are periodic Poisson processes. This model has been generalized here to allow for phase differences between the periodic inputs, which models a globular bushy cell (GBC) of the AVCN receiving AN fiber inputs originating over a spatial spread of the BM and therefore having differing phases. As a result, estimations of the spatial summation distance for which the SI of a GBC's response to a pure tone is enhanced, or degraded, relative to the SI of the input AN fibers' responses to a tone are made.

The neuron model is outlined in the Methods section, which also gives details of the inputs and how the spatial summation and integration are carried out. The Results section contains a description of how the output SI varies as a function of frequency and summation distance, both with and without introducing a general form of temporal jitter. In the Discussion section the results presented here are related to current understanding of the processing of information in the auditory pathway and their possible implications for cochlear implants.

2. Methods

2.1. Neural Model

The analysis presented here considers a single neuron with N independent inputs (afferent fibers) assumed to have the same synaptic response amplitude, a, and time

course, $s(t)$. The time course of an input at the site of spike generation is described by the synaptic response function $u(t)$ for the LIF neuron. The membrane potential is assumed to be reset to its initial value at time $t = 0$, $V(0) = v_0$, after a spike has been generated. A spike is produced only when the membrane potential exceeds the threshold, V_{th}, which has a potential difference with the reset potential of $\theta = V_{\text{th}} - v_0$. The potential is the sum of the EPSPs (Burkitt and Clark, 1999, 2000, 2001; Hohn and Burkitt, 2001)

$$V(t) = v_0 + N\,a\,s(t), \quad s(t) = \sum_{m=1}^{\infty} u(t - t_m), \quad (1)$$

where the index m denotes the mth input spike from the particular fiber, whose time of arrival is t_m $(0 < t_1 < t_2 < \cdots < t_m < \cdots)$. The rate of the input spike arrival times is discussed in the following section. The synaptic response function, $u(t)$, is given by the shot-noise response function

$$u(t) = \begin{cases} e^{-t/\tau} & \text{for } t \geq 0 \\ 0 & \text{for } t < 0, \end{cases} \quad (2)$$

where τ is the decay time constant of the membrane potential. Consequently, the membrane potential has a discontinuous jump of size a on the arrival of an EPSP and then decays exponentially between inputs. The decay of the EPSP across the membrane means that the contribution from EPSPs that arrive earlier has partially decayed by the time that later EPSPs arrive. In this study the voltage scale is set so that $v_0 = 0$ and $\theta = 1.0$.

2.2. *Spatial Integration of Inputs*

The input to GBCs provided by each AN fiber may be described by a periodic input spiking-rate function $\lambda(t)$ (chosen here to be a sum of identical Gaussian functions centered at multiples of the period), modeled as a periodic Poisson process (Kempter et al., 1998). In order to include a phase delay associated with the traveling wave stimulating consecutive AN fibers (labeled with a subscript n) over a spatial spread of the BM, the phase of the function $\lambda_n(t)$ must depend on the position of the fiber. As the sound-induced traveling wave moves from the base of the BM, where high frequencies are represented, to the apex of the BM, where low frequencies are represented, the AN fibers are consecutively stimulated. This gives rise to phase differences between the spiking-rate functions, $\lambda_n(t)$, of each input AN fiber, and these phase differences depend on the distance between the points of BM innervation of each AN fiber.

The same treatment of input frequency is employed as used in the study by Bruce et al. (1998), where each input fiber responds to a tone that is at the fiber's CF. Furthermore, it is assumed that each input fiber originates at the position on the BM corresponding to the CF of interest (i.e., at the CP), that the fibers all have the same conduction time (Paolini and Clark, 1998), and that the fibers have a high spontaneous rate (or equivalently a low-threshold). Thus the SI and spiking-rate of each input will be the same, and the phase of each input spiking-rate function depends on the CP. Moreover, this results in phase delays between inputs, $t_{\phi,n}$, that change linearly with slope α (called the phase-delay parameter) over small distances around the CP. For N identical fibers spread out evenly over distance d on the BM, the phase delay of the nth fiber can be expressed by $t_{\phi,n} = \alpha d n/N$ (Bruce et al., 1998), and thus the input spiking-rate function of the nth fiber is

$$\lambda_n(t) = p\left(\sum_{k=-\infty}^{\infty} \frac{1}{\sqrt{2\pi\sigma^2}} \times \exp\left(-\frac{\left(t - kT + t_\phi + \alpha d\,\frac{n}{N}\right)^2}{2\sigma^2}\right)\right), \quad (3)$$

where the time-dependent rate of arrival of input spikes at a synapse is periodic with period T and initial phase t_ϕ (i.e., the phase of the input at the time when the PSP summation commences), p is the time-averaged input spiking-rate per period, and σ is the standard deviation (SD) of the Gaussians. The SI of the above spiking-rate function, denoted R, is given by Kempter et al. (1998)

$$R = \exp\left(-\frac{2\pi^2\sigma^2}{T^2}\right). \quad (4)$$

This expression for R can be calculated by dividing the first complex Fourier coefficient of $\lambda_n(t)$ by the zeroth complex Fourier coefficient of $\lambda_n(t)$. The period and the SD of the Gaussians can be varied independently. The use of the term *period* (or *frequency* $f = 1/T$) here and throughout the analysis refers to this periodic modulation of the rate of inputs (and is not to be confused with the time averaged spiking-rate on each input fiber, which is $\bar{\lambda}_{\text{in}} = p/T$). This input spiking-rate function represents an inhomogeneous (i.e., nonstationary) Poisson process (Papoulis, 1991).

The treatment of neural spike trains as homogeneous Poisson processes provides a good approximation to spontaneous activity (Cox and Lewis, 1966; Perkel et al., 1967), as observed in AN fibers. Furthermore, the treatment of neural spike trains involved in temporal coding as periodic inhomogeneous Poisson processes has also been shown to provide a good approximation of AN fiber responses to tones (Johnson and Swami, 1983). The Poisson model presented here appears to be a reasonably accurate description of neural spike trains involved in temporal coding, with the only major shortcoming being the lack of refractory effects. However, this can be compensated for by reducing the input SI, R_{in}, for high frequencies where refractory effects are most noticeable. The above definition of SI, Eq. (4), allows the modeling of R_{in} values between zero and one (Kempter et al., 1998).

2.2.1. Integral Approximation of the Spatial Summation. The spatial summation of the activity of these N AN fibers over the distance d can be simplified, both analytically and computationally, by converting the input spiking-rate function, Eq. (3), into a continuous expression of spiking-rate per unit distance, $\lambda(x, t)$ (Bruce et al., 1998). Expressing $\lambda_n(t)$ in the spatially continuous (rate per unit distance) form, $\lambda(x, t)$, gives

$$\lambda(x,t) = \frac{pN}{d}\left(\sum_{k=-\infty}^{\infty} \frac{1}{\sqrt{2\pi\sigma^2}} \times \exp\left(-\frac{(t - kT + t_\phi + \alpha x)^2}{2\sigma^2}\right)\right), \quad (5)$$

where N/d is the nerve fiber density and x is the spatial variable. The spatial summation over the N evenly spread inputs can be approximated by the integration of the spiking-rate per unit distance function, $\lambda(x, t)$, over the distance $[0, d]$, for which it is assumed that the inputs are uniformly distributed. This integral approximation of the spatial summation of the spiking-rate functions of the AN fiber inputs, denoted $\hat{\lambda}(t)$, becomes

$$\hat{\lambda}(t) = \int_0^d dx\, \lambda(x,t). \quad (6)$$

Since $\hat{\lambda}(t)$ involves a bi-infinite sum of aperiodic functions, its evaluation can be quite computationally demanding when it is approximated with a finite number of terms. Instead, it is possible to approximate $\lambda(x, t)$ by using its Fourier series, given by

$$\lambda^F(x,t) = \frac{Np}{Td} + \frac{2Np}{Td}\left(\sum_{m=1}^{\infty} \exp\left(-\frac{2m^2\pi^2\sigma^2}{T^2}\right) \times \cos\left(\frac{2\pi m}{T}(t + t_\phi + \alpha x)\right)\right). \quad (7)$$

The resultant expression for $\hat{\lambda}(t)$ is then

$$\hat{\lambda}(t) = \frac{Np}{T} + \frac{Np}{\pi\alpha d}\sum_{m=1}^{\infty} \frac{\exp\left(-\frac{2m^2\pi^2\sigma^2}{T^2}\right)}{m} \times \left(\sin\left(\frac{2\pi m}{T}(t + t_\phi + \alpha d)\right) - \sin\left(\frac{2\pi m}{T}(t + t_\phi)\right)\right). \quad (8)$$

Consequently, $\hat{\lambda}(t)$ is approximated by an expression involving an infinite sum of periodic functions. Using $\lambda^F(x, t)$ it was found that the first 30 terms of $\hat{\lambda}(t)$ provided an accurate approximation for SI values up to and including 0.9 (this was half the number of terms required for a similar accuracy of $\hat{\lambda}(t)$ over the same SI range when the expression for $\lambda(x, t)$ in Eq. (5) was used).

2.2.2. The Input Population Synchronization. In order to understand the relative effects of spatial summation and temporal integration on the output synchronization, we first consider the input population synchronization, $\hat{R}_{\text{in}}$, which is the SI of the spiking-rate function of the spatially integrated synaptic input, $\hat{\lambda}(t)$—i.e., the SI of the arriving PSPs in a population of fibers,

$$\hat{R}_{\text{in}} = R_{\text{in}}\left|\left(\frac{T}{\pi\alpha d}\right)\sin\left(\frac{\pi\alpha d}{T}\right)\right|. \quad (9)$$

The input population synchronization, $\hat{R}_{\text{in}}$, is clearly less than the input synchronization on the individual fibers, R_{in}, since it involves the average over many such fibers with different phases (note that $\hat{R}_{\text{in}} \to R_{\text{in}}$ as $d \to 0$). The input population synchronization, $\hat{R}_{\text{in}}$, corresponds to the output synchronization, R_{out}, for the neuron model with an infinite membrane time constant, $\tau \to \infty$, also known as the perfect

integrate-and-fire model,

$$R_{\text{out}} \overset{\tau\to\infty}{\longrightarrow} \hat{R}_{\text{in}}. \tag{10}$$

This relationship follows by noting that in the perfect integrate-and-fire model the probability of crossing the spiking threshold is simply proportional to the instantaneous rate of the combined synaptic inputs (i.e., the sum total of the product of the individual input spiking-rates with their resulting PSP amplitudes), assuming that the PSPs are of equal amplitude (Burkitt and Clark, 2001). The perfect integrate-and-fire model also forms a good approximation in the situation where the average rate of synaptic input is very high, resulting in a temporal integration time that is effectively very much shorter than the membrane potential decay time constant. This limit therefore provides a lower bound on the output SI as the input rate increases. However, the perfect integrate-and-fire model is clearly incapable of enhancing the output SI relative to either the input SI on individual fibers, R_{in} or the input population SI, $\hat{R}_{\text{in}}$.

2.2.3. Upper Bound on the Error of the Integral Approximation. The main mathematical approximation of this spatiotemporal analysis is the integral approximation, Eq. (6), of the spatial summation of the spiking-rate functions of N input AN fibers. As shown explicitly by Bruce et al. (1998), this type of approximation becomes more accurate as the nerve fiber density, N/d, increases. Because we are interested in analyzing the spatial summation distance of AN fiber inputs to GBCs, AN fiber input densities as low as 40 cm^{-1} were used. The integral approximation is consequently expected to be more accurate for high frequency inputs where the spiking-rate expression for the nth fiber, Eq. (3), becomes flatter—which is a result of low input SIs, Eq. (4), and the maximum slope with respect to distance of the spiking-rate per unit distance expression, Eq. (5), being at its lowest values. An upper bound on the (normalized) relative difference between the integral approximation and the spatial summation is given in the Appendix (although this upper bound does not represent the lowest upper bound on the relative difference, it nevertheless still provides a constraint on the error of the integral approximation).

2.3. Output of the Model

Now that the neuron model and its synaptic inputs have been defined, the output of the model can be evaluated using the methods of Burkitt et al. (1999, 2000, 2001). Based on a description of the membrane potential and the spatially integrated synaptic inputs, the synaptic inputs can be temporally integrated and the probability density of the membrane potential $V(t)$ can be obtained in the Gaussian approximation (Kenyon et al., 1992; Burkitt and Clark, 1999). The probability density of the potential $V(t)$, denoted by $p(v, t \mid v_0; \omega, \phi)$, is the probability that the potential has the value v at time t, given that the initial condition is $V(0) = v_0$, the angular frequency of the input is ω (with $\omega = 2\pi f$), and the initial phase is ϕ (corresponding to an initial time t_ϕ with $\phi = 2\pi t_\phi$) (Burkitt and Clark, 2001). This initial condition corresponds to the reset of the membrane potential to v_0 immediately after the previous spike, which is assumed to occur at time $t = 0$. In the Gaussian approximation, the probability density can be written as

$$p(v, t \mid v_0; \omega, \phi) = \frac{1}{\sqrt{2\pi\Gamma(t; \omega, \phi)}} \times \exp\left\{-\frac{(v - v_0 - \Upsilon(t; \omega, \phi))^2}{2\Gamma(t; \omega, \phi)}\right\}, \tag{11}$$

where

$$\begin{aligned} \Upsilon(t; \omega, \phi) &= a \int_0^t \hat{\lambda}(t') u(t - t')\, dt', \\ \Gamma(t; \omega, \phi) &= a^2 \int_0^t \hat{\lambda}(t') u^2(t - t')\, dt'. \end{aligned} \tag{12}$$

The dependence of $\Upsilon(t; \omega, \phi)$ and $\Gamma(t; \omega, \phi)$ on angular frequency, ω, and initial phase, ϕ, is consequently given explicitly through their dependence on $\hat{\lambda}(t)$. In the above we have assumed for simplicity that both the amplitude, a, and time course, $u(t)$, of all input PSPs are identical. The Gaussian approximation, which takes its name from the Gaussian form of the expression for the membrane potential given in Eq. (11), may be derived by keeping only the terms to second order in the amplitude a of the postsynaptic potential (Kenyon et al., 1992; Burkitt and Clark, 1999, 2000), and consequently the approximation is expected to work best for small values of a (compared to the spiking threshold θ), which corresponds to large values of N.

In order to calculate the output spike-phase distribution (corresponding to the experimentally measured phase histogram), it is first necessary to calculate the conditional first-passage time density, $f_\theta(t; \omega, \phi)$, which is the distribution of interspike interval times (i.e., the times when the summed membrane voltage

crosses threshold, given that the previous spike occurred at time $t = 0$), dependent on the angular frequency and phase of the synaptic input. This conditional first-passage time density is evaluated using a generalization of the renewal equation (Plesser and Tanaka, 1997; Burkitt and Clark, 2000). In the calculation of the phase distribution of output spikes, a discretization of 40 time-steps per period was used (this ensures an accurate determination of the output SI over the range of values investigated here). An absolute refractory period was also introduced into the model (Burkitt and Clark, 2000). For increasing input frequencies and decreasing output spiking-rates the calculation of the conditional first-passage time densities results in an increasing number of required time-steps, which demands increasing computational resources.

The next step is to find the phase distribution of the output spikes, $\chi^{(s)}(\phi)$, which is also the distribution of initial phases of the conditional first-passage time density. This phase distribution is given by the stationary solution to a phase transition density (Plesser and Geisel, 1999; Burkitt and Clark, 2001), which is defined by the periodic wrapping of the conditional first-passage time densities with varying initial phases. It is then straightforward to calculate the output SI from the phase distribution.

Although the model used in this study accounts for stochastic temporal jitter in AN fiber responses to a pure tone, there are several forms of neural noise that have not been incorporated into the model. Such forms of noise include spontaneous inputs from fibers not associated with the stimulus, spike propagation delay time jitter in AN fibers (Anderson, 1973) and synaptic EPSP release time jitter (Walmsley et al., 1998). In order to account for these forms of neural noise an additional Gaussian neural noise term was introduced into the model. This was incorporated by convolving the output phase distribution of the model, $\chi^{(s)}(\phi)$, with a periodically wrapped Gaussian jitter function with standard deviation σ_J in the vicinity of the experimentally observed range of 50 to 110 μsec (Anderson, 1973; Paolini et al., 2001)

$$\chi^{(s)}_{\text{conv}}(\phi) = \int_0^{2\pi} d\phi' \chi^{(s)}(\phi') G(\phi - \phi'; \sigma_J), \qquad (13)$$

$$G(\phi; \sigma_J) = \sum_{k=-\infty}^{\infty} \frac{1}{\sigma_J \sqrt{2\pi}} \exp\left(-\frac{(\phi - 2k\pi)^2}{2\sigma_J^2} \right).$$

The effect of introducing this Gaussian neural noise is to smear the output spike-time distribution, resulting in a reduction of the degree of phase locking to high-frequency stimuli, and the results of this analysis are presented in Section 3.3.

3. Results

3.1. *Parameters for Modeling AN Fibers and Globular Bushy Cells*

The CN contains a number of different cell types that exhibit spatiotemporal summation of AN inputs, of which bushy cells are one such class. The terminals of many AN fibers form large endbulbs that are attached to the soma of bushy cells and that contain many synapses (Brawer et al., 1974; Cant and Morest, 1979). Bushy cells also exhibit exceptionally short membrane time constants that arise as a result of a low-threshold potassium conductance (approximately -70 mV) (Manis and Marx, 1991), which plays an important role in their ability to process temporal information (Oertel, 1983; Paolini et al., 1997). Two types of bushy cells with distinct morphologies have been described: spherical bushy cells (SBCs) in the anterior AVCN and GBCs in the posterior AVCN (Cant and Morest, 1979). In the spatiotemporal analysis presented in this study, the parameters of the LIF neurons were chosen to model those of GBCs. GBCs are characterized by an ovoid soma with predominantly one primary dendrite with extensive branches (Brawer et al., 1974; Tolbert and Morest, 1982; Smith and Rhode, 1987). GBCs receive input predominately from high spontaneously active, low threshold AN fibers (Liberman, 1991). These AN fibers terminate in the form of modified (small) endbulbs (Osen, 1969, 1970; Brawer and Morest, 1975). Measurements indicate that they have up to 52 terminals on the soma of GBCs (Ostapoff and Morest, 1991), although the number of AN fibers that these terminals come from is not known (Rouiller et al., 1986). By contrast, SBCs typically receive larger endbulb of Held (Osen, 1969, 1970; Cant and Morest, 1979; Ryugo and Fekete, 1982) input from only 1 to 3 AN fibers (Lorente de Nó, 1981; Sento and Ryugo, 1989), which means that the Gaussian approximation of the LIF neuron formulation used in this study does not provide a good model of the responses of SBCs (Burkitt and Clark, 2001).

The analysis presented here establishes the relationship between the output SI, R_{out} (and the normalized output SI, which is the output SI divided by the input SI—namely, $R_{\text{out}}/R_{\text{in}}$) with the stimulus frequency

($f = 500$, 1000, 2000, and 5000 Hz) and spatial summation distance (0 mm $\leq d \leq$ 5 mm, with a spatial resolution of 0.125 mm). The parameter values used for the AN fiber input in this study were chosen to be the same as those used by Bruce et al. (1998) with the exception of the input SI, R_{in}, values at $f = 500$ Hz and $f = 1000$ Hz (because the analytical form of their spiking-rate function did not allow input SIs greater than 0.5, whereas the expression in Eq. (3) allows larger values). This enables a direct comparison to be made between their results, in which there was a finite temporal integration window with no thresholding, and our results, which include both a finite temporal integration window and the thresholding mechanism for spike generation (our analysis also allows a comparison with a neuron model with an infinite temporal integration window—the perfect integrate-and-fire model).

In the present study, the summation distance, d, was varied while keeping the number of input fibers, N, constant, whereas in the study of Bruce et al. (1998), the summation distance, d, was varied while keeping the input fiber density, N/d, constant. Two values for the number of input fibers N were chosen: 20 and 40, which are comparable to the numbers seen for GBCs (Lorente de Nó, 1981; Sento and Ryugo, 1989; Ostapoff and Morest, 1991; Rothman et al., 1993; Rothman and Young, 1996). The AN fiber parameters are chosen to model high spontaneous rate, low threshold AN fibers (Liberman, 1991; Bruce et al., 1998). The input SI was estimated for a stimulus intensity of 60 dB SPL for AN fibers responding to each stimulus frequency from plots of the nonoscillatory (A_n) and oscillatory (B_n) input spiking rates versus normalized position on the BM that were produced using a cochlea/AN model (Neely and Kim, 1986; Meddis et al., 1990; Bruce et al., 1998). The A_n and B_n values corresponding to the CP of the stimulus frequency of interest were chosen. The required input SI, denoted R_{in}, was calculated using the expression (Bruce et al., 1998)

$$R_{\text{in}} = \frac{B_n}{2A_n}. \tag{14}$$

The width, σ, of the Gaussian functions in the input spiking-rate function is given using Eq. (4),

$$\sigma = \sqrt{\frac{T^2}{2\pi^2} \ln\left(\frac{1}{R_{\text{in}}}\right)}. \tag{15}$$

Values for the input SI, R_{in}, at the four frequencies investigated are given in Table 1, and the values for 2000 Hz and 5000 Hz are the same as those used by Bruce et al. (1998). The values of the phase-delay parameter, α, for each input frequency were determined by the slope at the corresponding CP of phase lag curves for BM vibrations at the frequencies investigated, which were produced using a cochlea model (Neely and Kim, 1986) and are the same values as used in Bruce et al. (1998) (values provided in Table 1). The parameter values used here correspond to those of the cat auditory system, which has a BM length of about 25 mm (Retzius, 1984; Neely and Kim, 1986).

Table 1. Values of the input SI, R_{in}, and the phase-delay parameter, α, at the four frequencies investigated.

Frequency (Hz)	500	1000	2000	5000
(Period (ms))	(2.0)	(1.0)	(0.5)	(0.2)
R_{in}	0.682	0.574	0.405	0.194
α (ms/cm)	−9.04	−6.02	−3.59	−1.71

The average spiking rate of each input per period, p, can be calculated from the plots of the nonoscillatory (A_n) and oscillatory (B_n) input spiking rates versus normalized position on the BM produced by the cochlear/AN model. The average spiking rate of each input per period is then given by

$$p = T(A_n + B_n). \tag{16}$$

However, for $f = 5$ kHz these plots provide an average spiking rate per input that is so low that the spiking rate of the output of the model neuron was unacceptably low. In order to avoid this problem, the average spiking rate of each input fiber was taken to be $\bar{\lambda}_{\text{in}} = 180$ spikes/s across all input frequencies. This value ensured that a sufficient output response could be calculated across all input frequencies. Furthermore, it meant that the same (input) EPSP amplitude could be used across all the frequencies investigated. The EPSP amplitudes chosen—namely, $a = 0.27$ (for $N = 20$ inputs, $\tau = 0.5$ ms), 0.1228 ($N = 20$ inputs, $\tau = 2$ ms), and 0.0656 ($N = 40$ inputs, $\tau = 2$ ms)—are the amplitudes for which the output spiking rate of the model is the same as the input spiking rate of the model for a nonmodulated input (i.e., $\lambda(x, t)$ constant). The values chosen for the temporal jitter, $\sigma_J = 0, 25, 50, 75, 100\,\mu$s cover the range observed for both AN fibers (Anderson, 1973) and bushy cells (Paolini et al., 2001). An absolute refractory period of 1 ms was used. These values for the LIF neuron and input parameters are summarized in Table 2 and represent values typical for GBCs

Table 2. Values of the remaining LIF neuron parameters and input parameters.

Number of inputs, N	20 & 40
EPSP amplitude, a	0.27, 0.1228, 0.0656
Average input spike rate on each fiber, $\bar{\lambda}_{\text{in}}$ (spikes/s)	180
Membrane potential decay time constant, τ (ms)	0.5 & 2.0
Absolute refractory period, τ_R (ms)	1.0
Threshold, θ	1.0
Temporal jitter, σ_{J} (μs)	0, 25, 50, 75, 100

(Rothman et al., 1993; Joris et al., 1994a; Zhang and Trussell, 1994; Rothman and Young, 1996).

3.2. *Enhancement of Synchronization*

This study looks at the effects of summation distance, d, and input frequency, f, on the SI of the output spikes, R_{out}, in the LIF neuron. Figure 1A is a plot of output SI, R_{out}, as a function of the summation distance, d, and input frequency, f, with $N = 20$ inputs, a membrane potential decay time constant of $\tau = 2$ ms, an input EPSP amplitude of $a = 0.1228$, a temporal jitter of $\sigma_{\text{J}} = 0$ μs, and the rest of the parameter values as given in Tables 1 and 2. The lines on the plot connect the points at which the output SI was evaluated. The figure shows a clear decrease in SI as the summation distance and input frequency increase. Bumps in the curve arise from a resonance between the phase differences (dependent on the α values) and the input period, T, with the minima corresponding to zeros in the input population synchronization, $\hat{R}_{\text{in}}$ (Eq. (9)). With an increase in input frequency, the width of these bumps decreases and the number of the bumps increases. Figure 1B is a plot, for the same parameter values as in Fig. 1A, of normalized output SI versus the summation distance, d, and the input frequency, f. In addition to the features evident in Fig. 1A, the figure shows that there is an *enhancement* of output SI relative to the input SI for short summation distances at all given input frequencies. It should also be noted that the enhancement of synchronization at $d = 0$ is greater for $f = 2000$ Hz than for frequencies below this value. This is because the output SI, R_{out}, saturates with an increase in the input SI, R_{in}, for the LIF neuron (Burkitt and Clark, 2001) and the input SI values studied here are larger at lower frequencies.

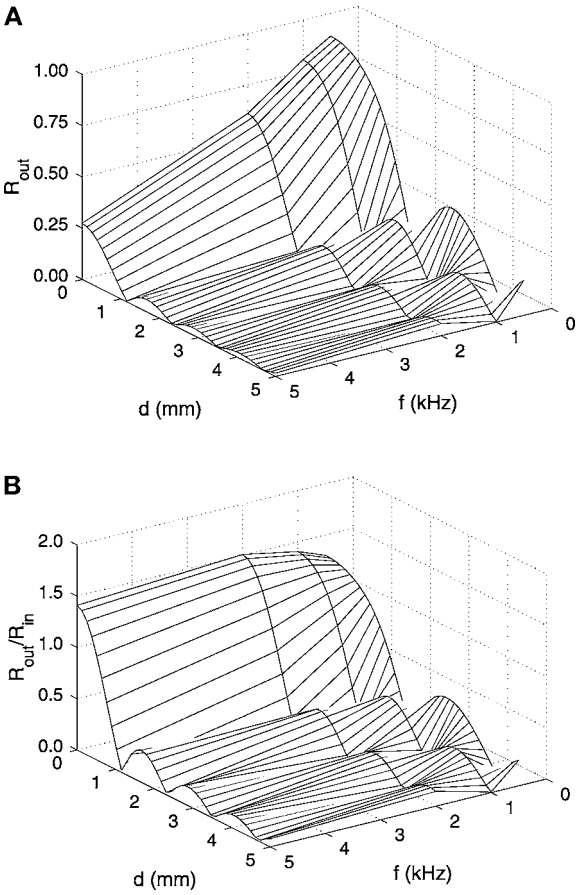

Figure 1. Plots of (**A**) output SI, R_{out}, and (**B**) normalized output SI, $R_{\text{out}}/R_{\text{in}}$, versus summation distance, d (in units of mm), and input frequency, f (in units of kHz). Parameter values are $N = 20$ inputs, $\tau = 2$ ms, $a = 0.1228$ and $\sigma_{\text{J}} = 0$ μs. All other parameters are as given in Tables 1 and 2. The lines on the plot connect the points at which the output SI was evaluated.

Upper bounds on the errors due to approximating the discrete spatial summation of the rate function by an integral, as shown in Eq. (6), are given in Table 3 (see the Appendix for details of the error calculation). The upper bound is roughly proportional to the summation distance, d, and inversely proportional to the number of inputs, N, so that the error is least for small summation distances and large numbers of inputs (the values in Table 3 are for $N = 20$). Although these values are relatively large, they represent an upper bound (not a lowest upper bound) on the error of the integral approximation, and the integral approximation is still expected to provide a good qualitative description of the effect of the spatial summation (which becomes better for larger N) and therefore is suitable for the purposes of this study.

Table 3. Upper bound on the error in the spiking-rate function due to approximating the spatial sum by an integral (values calculated for $N = 20$ and $M = 20$, see Appendix).

Spatial Summation Distance d (mm)	Frequency, f (Hz)			
	500	1000	2000	5000
0.1	17.3%	15.4%	10.4%	5.3%
0.2	34.6%	30.7%	20.7%	10.6%
0.3	52.0%	46.1%	31.1%	15.9%
0.4	69.3%	61.4%	41.5%	21.1%
0.5	86.6%	76.8%	51.9%	26.4%

Figure 2 shows the output SI, R_{out}, versus number of input fibers, N, for the Gaussian approximation (solid line), the spatially integrated input (dashed line), and the spatially summed input (dash-dotted line, which is almost coincident with the dashed line). The numerical simulations for the spatially integrated inputs (Eq. (8)) and the spatially summed inputs (Eq. (3)) in these plots represent averages over 20,000 output spikes. These results indicate that the Gaussian approximation is accurate in the large N limit. The difference between

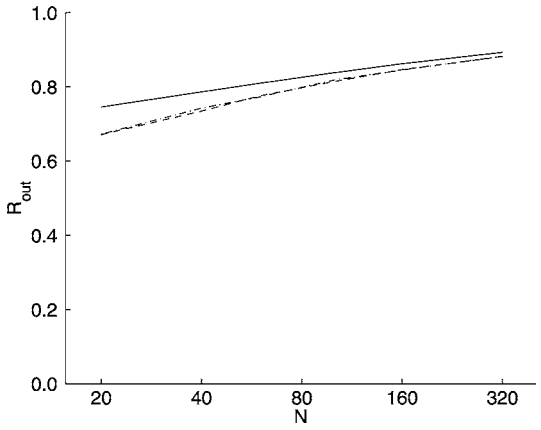

Figure 2. Plot of output SI, R_{out}, versus number of input fibers, N. The results for the Gaussian approximation (solid line) and the numerical simulations of both the spatially integrated input (dashed line) and the spatially summed input (dotted line) are shown. The spatially integrated input is described by Eq. (8) and the the spatially summed input is described by Eq. (3), with the N input fibers evenly distributed over the distance d. The parameters were as follows: $f = 1000$ Hz, $d = 0.513$ mm, $\tau = 2$ ms, $\lambda_{\text{in}} = 180$ spikes/s, $R_{\text{in}} = 0.574$, $\alpha = -6.02$ ms/cm, $\tau_R = 1$ ms, $\theta = 1$, $\sigma_j = 0$ s. The lines connect the results for individual points at the values $N = 20, 40, 60, 100, 160, 320$, with corresponding PSP amplitudes of $a = 0.1228, 0.0656, 0.0450, 0.0278, 0.0177, 0.0064$, respectively. Each numerical simulation represents results averaged over 20,000 output spikes.

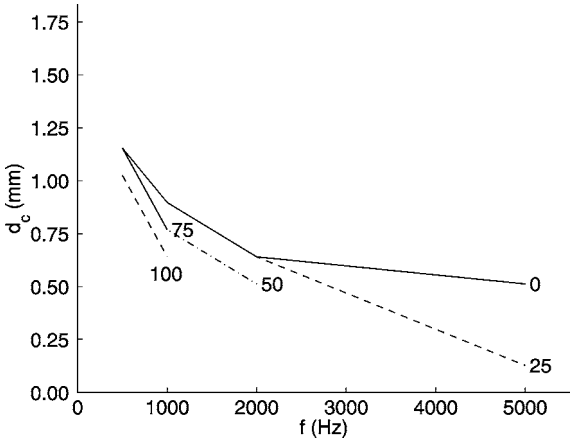

Figure 3. Plot of critical summation distance, d_{c} (in units of mm), required for synchronization enhancement versus input frequency, f (in units of kHz), in the presence of Gaussian noise with SDs of $\sigma_{\text{J}} = 0, 25, 50, 75, 100$ μs. (The uppermost plot corresponds to $\sigma_{\text{J}} = 0$ μs and the plots with successively greater slope correspond respectively to larger values of σ_{J} and are labeled accordingly.) The plot labeled 50 is partially obscured by that labeled 75. The remaining parameter values are the same as those in Fig. 1.

the results for the numerical simulations of the spatially integrated and the spatially summed expressions is negligible.

There is a critical summation distance, d_{c}, for each input frequency, below which synchronization is enhanced. The critical summation distance depends on frequency, and it corresponds to that part of the surface in Fig. 1B for which the normalized output SI, $R_{\text{out}}/R_{\text{in}}$, is greater than one. In Fig. 3 the uppermost plot (the solid line labeled 0) shows the critical summation distance, d_{c}, required for synchronization enhancement versus input frequency, f, corresponding to Fig. 1B (i.e., $\sigma_{\text{J}} = 0$ μs). As input frequency increases, the critical summation distance decreases (the remaining plots in Fig. 3 with nonzero temporal jitter are discussed in the following section).

The results of this analysis of the effects of spatiotemporal summation on GBC synchronization demonstrate both qualitatively and quantitatively (for the specific set of model parameter values used here) that phase differences between input AN fibers resulting from the traveling wave consecutively activating AN fibers originating over a spatial spread of the BM can either enhance or degrade the SI of the GBC's response relative to the SI of its input AN fibers. The degree of enhancement, or degradation, depends on these phase differences and thus also on the spatial spread of

the BM from which the input AN fibers originate (i.e., the summation distance, d).

In Fig. 1 the output response of the thresholding neuron shows a number of similarities with the output response of a summing (nonthresholding) neuron with similar parameter values, as studied by Bruce et al. (1998). Both models allow the output synchronization of the corresponding model neuron to be described as a function of the summation distance, d, over which input AN fibers originate, and the input frequency, f. Before the two models are compared, it is important to note some differences between the approaches used, apart from the major difference associated with thresholding (i.e., Bruce et al., 1998, did not include a spike-generation mechanism). First, the number of inputs to the thresholding neuron in this figure is fixed at 20, which is well within the range of inputs observed in GBCs of the AVCN (Lorente de Nó, 1981; Ostapoff and Morest, 1991), whereas Bruce et al. (1998) assumed a fixed nerve fiber density of 8570 cm^{-1}, resulting in a number of inputs that varies with summation distance. Second, the temporal integration of inputs was different for the two studies. The present study incorporated the summation of EPSPs that decayed with time (according to the membrane potential decay time constant), while the study of Bruce et al. (1998) incorporated a fixed temporal summation window without any decay. Third, in the present study only frequencies up to 5 kHz (instead of up to 10 kHz) were analyzed, since synchronization is observed to fall off well below this in almost all animals (Joris et al., 1994a; Oertel, 1999). Despite these differences, it is clear that the use of similar input parameters produces similar features in the responses of the two models, including the position of bumps resulting from a resonance between the input period and the phase differences. The most important difference is that the results for the summing neuron do not show an enhancement of synchronization (Bruce et al., 1998), which is seen in the present results and has been observed in GBCs (Joris et al., 1994a, 1994b; Köppl, 1997). The thresholding neuron shows the existence of a critical spatial summation distance for each input frequency, with spatial summation distances below this value giving an output SI that is greater than the input SI, as shown in Fig. 3. The values of the critical summation distances for each input frequency can be used to provide an upper bound on the length along the BM, about the CP, from which GBCs that display an enhancement of synchronization can receive afferent AN fiber input.

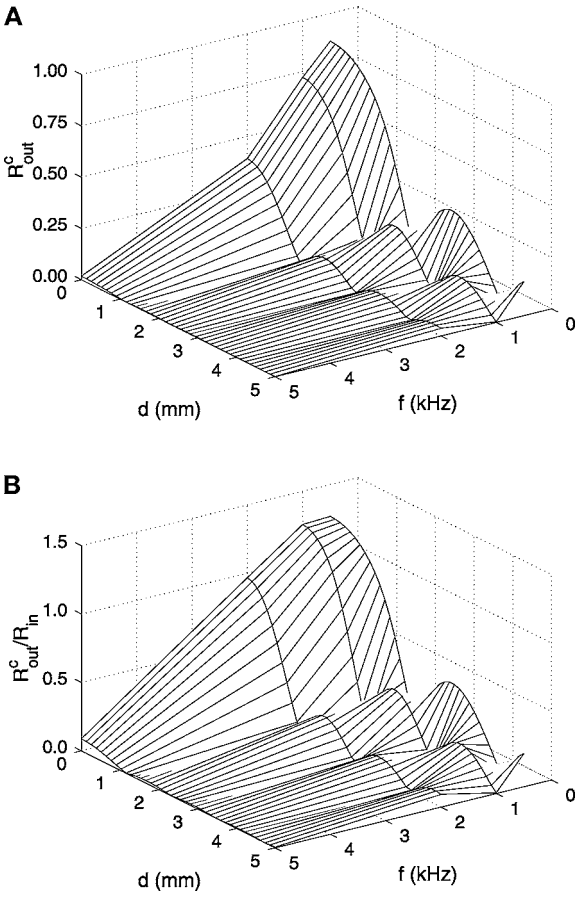

Figure 4. Plots of (**A**) convolved-output SI, R^c_{out}, and (**B**) normalized convolved-output SI, $R^c_{\text{out}}/R_{\text{in}}$, versus summation distance, d (in units of mm), and input frequency, f (in units of kHz), for a Gaussian noise with SD of $\sigma_J = 75$ μs and the same model parameter values as in Fig. 1. The lines on the plot connect the points at which the output SI was evaluated.

3.3. The Effects of Temporal Jitter

The results discussed in the previous section neglect the effect of stochastic temporal jitter in the neural response. Such jitter can be incorporated by convolving the output phase distribution with a periodically wrapped Gaussian function, as described in Section 2.3. Figure 4A is a plot of the convolved-output SI, R^c_{out} (i.e., the SI of $\chi^{(s)}_{\text{conv}}$ defined in Eq. (13)), as a function of the summation distance, d, and input frequency, f, for a Gaussian noise with a standard deviation of $\sigma_J = 75$ μs and the same model parameter values as in Fig. 1. Figure 4A demonstrates that the addition of temporal jitter to Fig. 1A reduces the SI of the output. This effect is greatest for higher frequencies,

where synchronization is almost completely removed. Figure 4B is a plot of the normalized convolved-output SI, $R^c_{\text{out}}/R_{\text{in}}$, as a function of the summation distance, d, and input frequency, f, for the same parameter values as in Fig. 4A.

The degree of temporal jitter in the auditory pathway varies across the different levels and cell types (Anderson, 1973; Walmsley et al., 1998) (see Section 2.3). The effect of this variability on the enhancement of synchronization in GBCs can be seen in Fig. 3, which shows plots of the critical summation distance, d_c, required for synchronization enhancement versus input frequency, f, in the presence of Gaussian noise (i.e., temporal jitter) with SDs of $\sigma_J = 0, 25, 50, 75, 100$ μs (The uppermost plot corresponds to $\sigma_J = 0$ μs and the plots with successively greater slope correspond respectively to larger values of σ_J and are labeled accordingly). The remaining parameter values are the same as those in Fig. 1. From Fig. 3 it is clear that an increase in the Gaussian noise term reduces the critical distance associated with the enhancement of synchronization, and the amount of reduction increases as frequency increases. Furthermore, when the SD of the Gaussian noise term is sufficiently large all enhancement of synchronization is removed, first at higher frequencies and then at lower frequencies as the temporal jitter increases. This effect is illustrated by the solid line labeled 75 in Fig. 3 (corresponding to $\sigma_J = 75$ μs and Fig. 4B), where an enhancement of synchronization is only seen for short summation distances at input frequencies of $f = 500$ Hz and $f = 1000$ Hz. Comparing this with the solid line labeled 0 in Fig. 3 (corresponding to $\sigma_J = 0$ μs and Fig. 1B), where enhancement of synchronization occurs for all frequencies when no Gaussian noise is present, it can be seen that a sufficiently large amount of temporal jitter prevents any enhancement of synchronization at input frequencies of $f = 2000$ Hz and $f = 5000$ Hz.

Apart from the variability in temporal jitter that can affect information processing in GBCs, there is also variability in the neuron parameters that constrain GBCs. Two GBC neuron parameters that vary between GBCs are the number of inputs N, which varies up to about $N = 50$ (Lorente de Nó, 1981; Sento and Ryugo, 1989; Ostapoff and Morest, 1991; Rothman et al., 1993; Rothman and Young, 1996), and the membrane potential decay time constant τ, which ranges from approximately $\tau = 0.2$ ms to $\tau = 8$ ms (Rothman et al., 1993; Joris et al., 1994a; Zhang and Trussel, 1994; Rothman and Young, 1996). Figure 5 shows the effects of varying either the number of inputs or the membrane potential decay time constant on the critical distance required for an enhancement of synchronization. All plots shown correspond to responses when a Gaussian noise with a SD of $\sigma_J = 75$ μs is present. The plot A in Fig. 5 corresponds to $N = 20$ inputs, a membrane potential decay time constant of $\tau = 2$ ms and an input EPSP amplitude of $a = 0.1228$. Plot B corresponds to $N = 40$ inputs, a membrane potential decay time constant of $\tau = 2$ ms and an input EPSP amplitude of $a = 0.0656$. Plot C corresponds to $N = 20$ inputs, a membrane potential decay time constant of $\tau = 0.5$ ms and an input EPSP amplitude of $a = 0.27$. The remaining parameter values are the given in Tables 1 and 2. Comparison of plots A and B indicates that an increase in the number of inputs (and a decrease in the EPSP amplitude), while the membrane potential decay time constant remains fixed, causes an increase in the critical distance for an enhancement of synchronization. This occurs because an increase in the number of inputs makes the membrane potential response to the input modulation less variable (Burkitt and Clark, 2001), thus increasing the SI of the output spikes and allowing larger values of the summation distance, d, that give an enhancement of synchronization. Comparison of plots A and C in Fig. 5 indicates that a decrease of the membrane potential decay time constant (and an increase in the EPSP amplitude), while

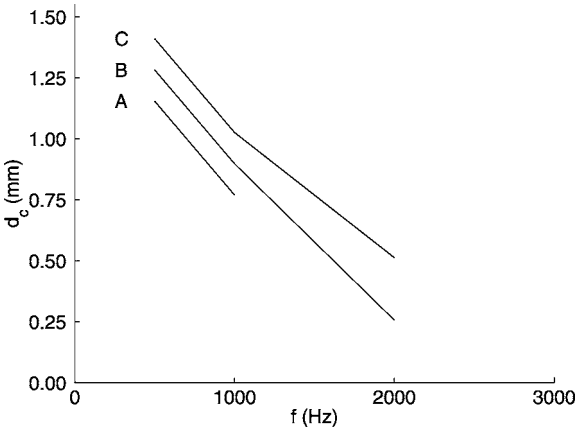

Figure 5. Plot of critical summation distance, d_c (in units of mm), required for synchronization enhancement versus input frequency, f (in units of kHz), when a Gaussian noise with a SD of $\sigma_J = 75$ μs is present and **A:** $N = 20$ inputs, $\tau = 2$ ms and $a = 0.1228$, **B:** $N = 40$ inputs, $\tau = 2$ ms and $a = 0.0656$, **C:** $N = 20$ inputs, $\tau = 0.5$ ms and $a = 0.27$. The remaining parameter values are the same as those in Fig. 4.

the number of inputs is fixed, causes an increase in the critical distance for an enhancement of synchronization. This occurs because a decrease of the membrane potential decay time constant improves the coincidence detection properties of the model, thus increasing the SI of the output spikes and allowing larger values of the summation distance, d, that give an enhancement of synchronization. The value $\sigma_J = 75$ μs in Figs. 4 and 5 for the SD of the Gaussian neural noise was chosen because (as seen in Figs. 3 and 5) it produces an enhancement of synchronization only in the range of frequencies (i.e., $f \leq 1 - 2$ kHz) at which enhancement of synchronization is seen in real GBCs (Joris et al., 1994a, 1994b).

Enhancement of synchronization in the present model arises because of the model's short membrane potential decay time constant (for the analysis presented here values of $\tau = 2$ ms and 0.5 ms were chosen) that produces short EPSPs. Furthermore, given that each of the EPSPs are subthreshold, the model neuron is likely to spike only when EPSPs have similar phases and coincidence detection occurs. The phase differences between the arrival of EPSPs are proportional to the spatial summation distance. As spatial summation distance decreases, so too do the phase differences. For a large spatial summation distance, EPSPs are out of phase, and the model neuron is less likely to spike at any particular phase of the input period. Thus, the output of the model neuron will be less synchronized than its inputs. On the other hand, as spatial summation distance is decreased there will be a spatial summation distance below which the EPSPs will be sufficiently in phase with one another, such that the synchronization of the membrane potential to the input period, in combination with the thresholding of the membrane potential, will lead to an enhancement of the output SI relative to the input SI. The addition of Gaussian noise, although convolved with the output of the LIF neuron, can effectively be thought of as being the result of random temporal fluctuations that are present in both the input spatiotemporal summation process described above as well as in the thresholding process of the LIF neuron. Thus comparing Fig. 1 with Fig. 4 it can be seen that the addition of such temporal jitter will have a greater smearing effect on temporal structure at high frequencies than at low frequencies. This will result in a greater reduction in the output SI at high frequencies than at low frequencies. Furthermore, the addition of temporal jitter, as is seen in Figs. 3 and 5, restricts the enhancement of synchronization in the present model to low frequencies.

4. Discussion

In order to model the synaptic input of neurons in the auditory pathway, it is necessary to consider the spatiotemporal patterns of activation caused by the traveling wave of the BM. This introduces spatially dependent phase differences to the periodic input of tonotopically organized neurons. The results presented here show the differing roles played by the spatial summation, which causes a decrease in the synchronization of the output as the spatial summation distance d increases, and the temporal summation, which causes an enhancement of the output synchronization through coincidence detection when the membrane potential decay time constant τ is small. In this study we have analyzed how these two contrasting effects depend on both the input (stimulus) and neuron parameters. Such considerations will be important for understanding how the auditory system processes more complex stimuli such as speech (Greenberg, 1996).

The use of the LIF neuron presented in this study as an approximation of GBCs can be justified on several grounds. First, the termination of modified endbulbs from AN fibers directly onto the soma of GBCs (Osen, 1969, 1970; Brawer and Morest, 1975; Rouiller et al., 1986; Ostapoff and Morest, 1991) is approximated well by the point nature of the LIF neuron, where input terminals arrive directly at the point of action potential generation. Second, the description of AN fiber inputs by inhomogenous Poisson processes provides a description of the stochastic nature of AN fiber spiking (Johnson and Swami, 1983). Furthermore, the model provides a small set of parameters that can be fitted (albeit only approximately) to existing experimental data for GBCs. However, there are a number of simplifications to realistic GBCs that the model presented here makes. One such important factor that has not been included in the model is the inhibitory inputs GBCs receive (Adams and Mugnaini, 1987; Saint-Marie et al., 1989), since not enough is known about their number, amplitude, and time course to include them in a useful way. These inhibitory inputs, however, have been shown to enhance the frequency tuning of GBCs (Paolini et al., 1998). Another important simplification is that the model assumes that the EPSPs are all of equal amplitude and time course,

whereas on a realistic neuron it is possible that the inputs on the dendritic tree and the soma have quite different amplitudes (and possibly also different time courses). Likewise, differences in the average input spiking rates are ignored, which is equivalent to assuming that all input fibers have the same threshold. The model also assumes that the input distribution is well characterized by the input spiking rate and input SI, which entails that more complex input distributions, such as peak splitting (Kiang and Moxon, 1972; Johnson, 1980; Palmer and Russell, 1986; Ruggero et al., 1986; Kiang, 1990; Joris and Yin, 1992; Ruggero et al., 1995; Cai and Geisler, 1996; Kuhlmann et al., 2001), are ignored.

Another assumption in the AN/GBC model of this study is that the AN fiber inputs all have the same average conduction delays. This approximation is supported by the work of Paolini and Clark (1998), in which intracellular recordings of the membrane potential of rat GBCs were made while AN fibers were electrically stimulated at their BM terminations. A single EPSP from a single AN fiber could be evoked in the membrane potential of the GBC using a small electric current. Increasing the amount of electrical stimulation resulted in the recruitment of more AN fibers that provided input to the GBC. It was found that increasing the amount of electrical stimulation did not significantly alter the position of the poststimulation peak of the membrane potential (which is the sum of the individual EPSPs from the various input fibers) indicating that all the EPSPs arrived at the GBC at approximately the same time. Furthermore, even if conduction delays are not uniform, the effect of their variance on the spatiotemporal summation presented in this analysis is likely to be much less significant than the effects of the slope of the phase-delay function, α, which is very steep in all cases of this analysis (see Table 1) and consequently produces significant phase delays across a small spatial spread of the BM. The temporal jitter incorporated into the model of this study is expected to account for the variability about the mean of the conduction delays (Anderson, 1973) but cannot account for fixed differences in the mean conduction delays across AN fibers.

The bumps observed in the output SI, R_{out}, in Figs. 1 and 4 result from a resonance between the phase differences and the period, with minima corresponding to zeros in the input population synchronization, $\hat{R}_{\text{in}}$ (Eq. (9)), when there are equal inputs from all phases. This resonance arises as a consequence of considering a uniform distribution of the inputs over the distance d, as can be seen from Eq. (9), where the input population synchronization $\hat{R}_{\text{in}}$ is zero when d is a multiple of T/α, irrespective of the input synchronization R_{in} on the individual fibers (this equation also describes the reduction in amplitude of successive maxima as d increases in Figs. 1 and 4). This uniform distribution was chosen in order to facilitate the comparison with existing results (Bruce et al., 1998). It is quite possible, however, to consider distributions of inputs different from Eq. (6), and another natural choice is the Gaussian distribution, for which

$$\hat{\lambda}(t) = \int \frac{dx}{\sqrt{2\pi d^2}} \lambda(x,t) \exp\left\{ -\frac{x^2}{2d^2} \right\}. \qquad (17)$$

The relationship between the input synchronization and the input population synchronization in this case is

$$\hat{R}_{\text{in}} = R_{\text{in}} \exp\left\{ -\frac{2\pi^2\alpha^2 d^2}{T^2} \right\}, \qquad (18)$$

which shows a gradual decrease as d increases.

The results of this analysis significantly highlight the presence of noise in the processing of AN fiber inputs by GBCs. In the model *without* temporal jitter, illustrated in Fig. 1B, it is clear that at high frequencies ($f = 2000$ Hz and $f = 5000$ Hz) there is an enhancement of synchronization of the output SI relative to the input SI. However, electrophysiology demonstrates that there is a degradation of synchronization in GBCs at these frequencies (Joris et al., 1994a, 1994b). The addition of Gaussian noise ($\sigma_J = 75$ μs) produces an enhancement of synchronization only at $f = 500$ Hz and $f = 1000$ Hz, as seen in Fig. 4B, which is in agreement with electrophysiology (Joris et al., 1994a, 1994b). Future studies will be aimed at elucidating the sources of this noise, which could specifically include spike propagation delay time jitter in AN fibers (Anderson, 1973) and synaptic EPSP release time jitter (Walmsley et al., 1998), as mentioned in Section 2.3. The use of compartmental models could also be fruitful in such an analysis (Rothman et al., 1993; Rothman and Young, 1996).

The critical distances presented in Figs. 3 and 5, although they are only upper bounds on the summation distances required for enhancement of synchronization across CF, still demonstrate the possibility that AN fiber inputs to a given GBC could originate

from a comparatively large spatial spread of the BM. The ability for GBCs (i.e., the LIF neuron) to produce an enhancement of synchronization under these conditions indicates the robustness of the temporal coding abilities of GBCs. A further point to note from Figs. 3 and 5 is that the critical distance appears to decay exponentially with an increase in input frequency. This indirectly supports the notion that the actual summation distance as a function of the CF of GBCs decreases exponentially with an increase in CF. By studying the responses of GBCs to high-intensity 500 Hz tones, Joris et al. (1994b) have demonstrated that GBCs with high CFs respond with a greater enhancement of synchronization relative to the responses of AN fibers with high CFs than the enhancement of synchronization seen in the responses of GBCs with low CFs relative to the responses of AN fibers with low CFs. This provides indirect evidence that the actual summation distance over which AN fibers (that provide the GBC input) originate on the BM decreases with the CF of the AN fibers and the GBCs. It would be hoped that future modeling studies could investigate the actual summation distance over which the AN fibers originate as a function of the CF of GBCs when more accurate parameters are available from experimental studies. An important point to consider in such modeling studies will be the actual range of CFs represented by the AN fiber inputs to a given GBC (Carney, 1990; Carney and Friedman, 1998). Thus future work could apply a generalization of the spatiotemporal summation analysis presented in this study to the modeling of the responses of CN neurons that receive AN fiber inputs over a broad range of CFs—e.g., stellate cells or octopus cells in the ventral CN (Rhode and Smith, 1986; Carney, 1990). This type of modeling could have implications for sound intensity coding in the CN (Evans, 1981; Rhode and Smith, 1986; May and Sachs, 1992; Carney, 1994) or for the coding and detection of spatiotemporal features of the AN response to a complex sound in the responses of AVCN neurons (Carney, 1990, 1992, 1994; Carney and Friedman, 1998).

The analysis presented here may have implications for cochlear implants. One of the key factors in the performance of cochlear implants is the degree of current spread from the stimulating electrodes (see Clark, 1996, 1999) and Loizou (1999) for reviews on cochlear implants). The critical summation distances, presented in Figs. 3 and 5, provide an indication of the spatial resolution of the current spread necessary in order that the GBC response to electrical stimulation from a cochlear implant be comparable to their response with acoustical stimulation (i.e., to enhance synchronization in GBCs relative to the synchronization of input AN fibers for each input frequency). Present electrical stimulation paradigms only coarsely approximate the spatiotemporal pattern of activation of AN fibers that occurs with acoustical stimulation in normal hearing. In particular, a pulse from a single implant electrode typically generates APs in neighboring AN fibers that are highly synchronized and have little temporal jitter (Clark et al., 1995). As a result, present stimulation paradigms do not mimic the way in which the traveling wave activates AN fibers. Nevertheless, future developments in electrode array design may provide sufficiently fine spatial resolution that the stimulation of consecutive electrodes could mimic the traveling wave activation of AN fibers and CN neurons that are generated by acoustical stimulation.

5. Conclusions

The results presented in this study show how LIF neurons receiving periodic input respond when the phases of the inputs vary with their spatial location. The analysis shows how the temporal information contained in the output spikes—namely, the output SI, depends on the spatial summation distance of the periodic stochastic inputs, as well as the details of the LIF neuron model (number of inputs N, EPSP amplitude a, threshold θ, membrane potential decay time constant τ, and temporal jitter σ_J) and the details of the periodic input (frequency f, input synchronization R_{in}, average spiking rate per period for each input fiber p, phase-delay parameter α, and analytical form of the periodic spiking rate function $\lambda_n(t)$). As a model of GBCs in the AVCN, it enables an upper bound on the degree of spatial spread (i.e., the summation distance d) on the BM from which their AN fiber inputs originate to be deduced. This neural model for spatiotemporal summation provides insight into the relationship between the various model parameters and the temporal properties of the output spikes. In particular, the analysis elucidates the different effects on the output caused by the spatial summation, which reduces the output synchronization, and by temporal integration, which increases the output synchronization through coincidence detection. The model also shows under what conditions (i.e., amount of temporal jitter) an enhancement of

synchronization, such as observed for GBCs (Joris et al., 1994a), will occur for low frequencies of acoustical stimulation.

Appendix: The (Normalized) Relative Difference Between the Integral Approximation and the Spatial Summation

The spatial analysis presented here (Section 2.2) considers N input AN fibers, each defined by the spiking-rate function, $\lambda_n(t)$ Eq. (3). The spatial summation of these N input AN fibers, denoted $\lambda^S(t)$, is therefore defined as

$$\lambda^S(t) = \sum_{n=1}^{N} \lambda_n(t). \tag{19}$$

The integral approximation of the above spatial summation, denoted $\hat{\lambda}(t)$, is given by Eq. (6). The (normalized) relative difference between $\hat{\lambda}(t)$ and $\lambda^S(t)$ provides a upper bound on the error of the integral approximation.

Following the method of Bruce et al. (1998) and letting the absolute difference between $\hat{\lambda}(t)$ and $\lambda^S(t)$ be defined as β gives

$$\left\| \int_0^d dx\, \lambda(x,t) - \sum_{n=1}^{N} \lambda_n(t) \right\| = \beta. \tag{20}$$

Replacing $\lambda(x,t)$ with its Fourier Series, denoted $\lambda^F(x,t)$ Eq. (7), and multiplying both sides by d/N gives

$$\left\| \frac{d}{N} \int_0^d dx\, \lambda^F(x,t) - \sum_{n=1}^{N} \frac{d}{N} \lambda_n(t) \right\| = \frac{d}{N}\beta. \tag{21}$$

The left-hand side of Eq. (21) is the difference between the integral over distance d of a function continuous in space and the sum of N rectangles each of height $\lambda_n(t)$ and width d/N. The greatest relative difference will occur where the absolute slope of the spiking rate $\lambda^F(x,t)$ is at a maximum. The absolute slope of $\lambda^F(x,t)$ is bound by

$$\left\| \frac{\delta \lambda^F(x,t)}{\delta x} \right\| \le \left\| \frac{4\pi p \alpha}{T^2} \sum_{m=1}^{\infty} m(R_{\text{in}})^{m^2} \right\|. \tag{22}$$

Since there is no known finite expression for $\sum_{m=1}^{\infty} m(R_{\text{in}})^{m^2}$, the lowest upper bound on the relative difference between the integral approximation and the spatial summation cannot be determined analytically. However, it is possible to obtain a useful upper bound by noting that the sum converges very quickly for the values of R_{in} we use. Consequently, we explicitly sum the first M terms ($M = 20$ is sufficient) and use the bound $\sum_{m=M}^{\infty} m(R_{\text{in}})^{m^2} \le \sum_{m=M}^{\infty} m(R_{\text{in}})^{m}$ (for $R_{\text{in}} < 1$). An upper bound in the absolute slope of $\lambda^F(x,t)$ exists as follows

$$\begin{aligned} &\left\| \frac{\delta \lambda^F(x,t)}{\delta x} \right\| \\ &\quad \le \left\| \frac{4\pi p \alpha}{T^2} \left(\sum_{m=1}^{M} m(R_{\text{in}})^{m^2} + \sum_{m=M+1}^{\infty} m(R_{\text{in}})^{m} \right) \right\| \\ &\quad = \left\| \frac{4\pi p \alpha}{T^2} \left(\sum_{m=1}^{M} m(R_{\text{in}})^{m^2} \right.\right. \\ &\qquad \left.\left. + \frac{(M+1)(R_{\text{in}})^{M+1} - M(R_{\text{in}})^{M+2}}{(1-R_{\text{in}})^2} \right) \right\|. \end{aligned} \tag{23}$$

Therefore, by summing the upper bounded errors of the individual rectangles and then dividing by the mean of $\hat{\lambda}(t)$, denoted $\langle \hat{\lambda} \rangle$, an upper bound on the normalized relative difference between the integral approximation and the spatial summation can be obtained,

$$\begin{aligned} &\left\| \frac{\hat{\lambda}(t) - \lambda^S(t)}{\langle \hat{\lambda} \rangle} \right\| \\ &\quad \le \left\| \frac{2\pi \alpha d}{NT} \left(\sum_{m=1}^{M} m(R_{\text{in}})^{m^2} \right.\right. \\ &\qquad \left.\left. + \frac{(M+1)(R_{\text{in}})^{M+1} - M(R_{\text{in}})^{M+2}}{(1-R_{\text{in}})^2} \right) \right\|. \end{aligned} \tag{24}$$

Acknowledgments

This work was funded by the Bionic Ear Institute and the National Health and Medical Research Council of Australia (NHMRC, Project Grant #990816). We thank Ian Bruce for providing the values of the parameters used in Bruce et al. (1998).

References

Adams JC, Mugnaini E (1987) Patterns of glutamate decarboxylase immunostaining in the feline cochlear nuclear complex studied with silver enhancement and electron microscopy. J. Comp. Neurol. 262: 375–401.

Anderson DJ (1973) Quantitative model for the effects of stimulus frequency upon synchronization of auditory nerve discharges. J. Acoust. Soc. Am. 54: 361–364.

Bose A, Booth V, Reece M (2000) A temporal mechanism for generating the phase precession of hippocampal place cells. J. Comput. Neurosci. 9: 5–30.

Brawer JR, Morest DK (1975) Relations between auditory nerve endings and cell types in the cat's anteroventral cochlear nucleus seen with the Golgi method and Nomarski optics. J. Comp. Neurol. 160: 491–506.

Brawer JR, Morest DK, Kane EC (1974) The neuronal architecture of the cochlear nucleus of the cat. J. Comp. Neurol. 155: 251–300.

Bruce IC, Irlicht LS, Clark GM (1998) A mathematical analysis of spatiotemporal summation of auditory nerve firings. Inform. Sciences 111: 303–334.

Buonomano DV, Mauk MD (1994) Neural network model of the cerebellum: Temporal discrimination and the timing of motor reponses. Neural Comput. 6: 38–55.

Burkitt AN, Clark GM (1999) Analysis of integrate-and-fire neurons: Synchronization of synaptic input and spike output in neural systems. Neural Comput. 11: 871–901.

Burkitt AN, Clark GM (2000) Calculation of interspike intervals for integrate-and-fire neurons with poisson distribution of synaptic inputs. Neural Comput. 12: 1789–1820.

Burkitt AN, Clark GM (2001) Synchronization of the neural response to noisy periodic synaptic input. Neural Comput. 13: 2639–2672.

Cai Y, Geisler CD (1996) Temporal patterns of the responses of auditory-nerve fibers to low-frequency tones. Hearing Res. 96: 83–93.

Cant NB, Morest DK (1979) Organization of the neurons in the anterior division of the anteroventral cochlear nucleus of the cat: Light-microscopic observations. Neurosci. 4: 1909–1923.

Cant NB, Morest DK (1979) The bushy cells in the anteroventral cochlear nucleus of the cat: Study with the electron-microscope. Neurosci. 4: 1925–1945.

Carney LH (1990) Sensitivities of cells in the anteroventral cochlear nucleus of cat to spatio-temporal discharge patterns across primary afferents. J. Neurophysiol. 64: 437–456.

Carney LH (1992) Modelling the sensitivity of cells in the anteroventral cochlear nucleus to spatiotemporal discharge patterns. Phil. Trans. R. Soc. Lond. B336: 403–406.

Carney LH (1994) Spatiotemporal encoding of sound level: Models for normal encoding and recruitment of loudness. Hearing Res. 76: 31–44.

Carney LH, Friedman M (1998) Spatiotemporal tuning of low-frequency cells in the anteroventral cochlear nucleus. J. Neurosci. 18: 1096–1104.

Carr CE, Konishi M (1990) A circuit for detection of interaural time differences in the brain stem of the barn owl. J. Neurosci. 10: 3227–3246.

Clark GM (1996) Electrical stimulation of the auditory nerve: The coding of frequency, the perception of pitch, and the development of cochlear implant speech processing strategies for profoundly deaf people. Clin. Exp. Pharmacol. Physiol. 23: 766–776.

Clark GM (1999) Cochlear implants in the third millennium. Am. J. Otol. 20: 4–8.

Clark GM, Carter TD, Maffi CL, Shepherd RK (1995) Temporal coding of frequency: Neuron firing probabilities for acoustic and electrical stimulation of the auditory nerve. Ann. Otol. Rhinol. Laryngol. 104 (Suppl. 166): 109–111.

Colburn HS, Han Y, Culotta CP (1990) Coincidence model of MSO responses. Hearing Res. 49: 335–346.

Cox DR, Lewis PAW (1966) The Statistical Analysis of Series of Events. Methuen, London.

Eggermont JJ, Aertsen AMJH, Johannesma PIM (1983) Quantitative characterisation procedure for auditory neurons based on the spectro-temporal receptive field. Hearing Res. 10: 167–190.

Evans EF (1981) The dynamic range problem: Place and time coding at the level of the cochlear nerve and nucleus. In: J Syka, LM Atkins, eds. Neuronal Mechanisms and Hearing. Plenum, New York. pp. 69–85.

Galambos R, Davis H (1943) The response of single auditory-nerve fibers to acoustic stimulation. J. Neurophysiol. 6: 39–57.

Gerstner W, Kempter R, van Hemmen JL, Wagner H (1996) A neuronal learning rule for sub-millisecond temporal coding. Nature 383: 76–78.

Goldberg JM, Brown PB (1969) Response of binaural neurons of dog superior olivary complex to dichotic tonal stimuli: Some physiological mechanisms of sound localization. J. Neurophysiol. 32: 613–636.

Greenberg S (1996) Auditory processing of speech. In: NJ Lass, ed. Principles of Experimental Phonetics. Mosby, St. Louis. pp. 362–407.

Hohn N, Burkitt AN (2001) Shot noise in the leaky integrate-and-fire neuron. Phys. Rev. E 63: 031902.

Hubel D, Wiesel T (1962) Receptive fields, binocular interaction, and functional architecture in the cat's visual cortex. J. Physiol. 160: 106–154.

Jeffress LA (1948) A place theory of sound localization. J. Comp. Physiol. 41: 35–39.

Johnson DH (1980) The relationship between spike rate and synchrony in responses of auditory-nerve fibers to single tones. J. Acoust. Soc. Am. 68: 1115–1122.

Johnson DH, Swami A (1983) The transmission of signals by auditory-nerve fiber discharge patterns. J. Acoust. Soc. Am. 74: 493–501.

Joris PX, Carney LH, Smith PH, Yin TCT (1994a) Enhancement of neural synchronization in the anteroventral cochlear nucleus. I. Responses to tones at the characteristic frequency. J. Neurophysiol. 71: 1022–1036.

Joris PX, Smith PH, Yin TCT (1994b) Enhancement of neural synchronization in the anteroventral cochlear nucleus. II. Responses in the tuning curve tail. J. Neurophysiol. 71: 1037–1051.

Joris PX, Smith PH, Yin TCT (1998) Coincidence detection in the auditory system: Fifty years after Jeffress. Neuron 21: 1235–1238.

Joris PX, Yin TCT (1992) Responses to amplitude-modulated tones in the auditory nerve of the cat. J. Acoust. Soc. Am. 91: 215–232.

Kalluri S (2000) Cochlear nucleus onset neurons studied with mathematical models. Ph.D. thesis, Harvard-MIT Division of Health Sciences and Technology, Massachusetts Institute of Technology, Cambridge, MA.

Kempter R, Gerstner W, van Hemmen JL, Wagner H (1998) Extracting oscillations: Neuronal coincidence detection with noisy periodic spike input. Neural Comput. 10: 1987–2017.

Kenyon GT, Puff RD, Fetz EE (1992) A general diffusion model for analyzing the efficacy of synaptic input to threshold neurons. Biol. Cybern. 67: 133–141.

Kiang NYS (1990) Curious oddments of auditory-nerve studies. Hearing Res. 49: 1–16.

Kiang NYS, Moxon EC (1972) Physiological considerations in artificial stimulation of the inner ear. Ann. Otol. 81: 714–730.

Kiang NYS, Watanabe T, Thomas EC, Clark LF (1965) Discharge Patterns of Single Fibers in the Cat's Auditory Nerve. MIT Press, Cambridge, MA.

Köppl C (1997) Phase locking to high frequencies in the auditory nerve and cochlear nucleus magnocellularis of the barn owl. J. Neurosci. 17: 3312–3321.

Kuhlmann L, Burkitt AN, Clark GM (2001) Peak-splitting in the response of the leaky integrate-and-fire neuron model to low frequency periodic input. In: B Lithgow, I Cosic, eds. Proceedings of Biomedical Research in 2001. Victorian Chapter IEEE EMBS, Melbourne, pp. 13–16.

Lavine RA (1971) Phase-locking in the response of single neurons in cochlear nuclear complex of the cat to low-frequency tonal stimuli. J. Neurophysiol. 34: 467–483.

Liberman MC (1982) The cochlear frequency map for the cat: Labeling auditory-nerve fibers of known characteristic frequency. J. Acoust. Soc. Am. 72: 1441–1449.

Liberman MC (1991) Central projections of auditory-nerve fibers of differing spontaneous rate. I. Anteroventral cochlear nucleus. J. Comp. Neurol. 313: 240–258.

Loizou PC (1999) Introduction to cochlear implants. IEEE Eng. Med. Bio. Mag. 18: 32–42.

Lorente de Nó R (1981) The Primary Acoustic Nuclei. Raven Press, New York.

Manis PB, Marx SO (1991) Outward currents in isolated ventral cochlear nucleus neurons. J. Neurosci. 11: 2865–2880.

Maršálek P, Koch C, Maunsell J (1997) On the relationship between synaptic input and spike output jitter in individual neurons. Proc. Natl. Acad. Sci. USA 94: 735–740.

May BJ, Sachs MB (1992) Dynamic range in neural rate responses in the ventral cochlear nucleus of awake cats. J. Neurophys. 68: 1589–1602.

Meddis R, Hewitt MJ, Shackleton TM (1990) Implementation details of a computation model of the inner-hair cell/auditory-nerve synapse. J. Acoust. Soc. Am. 87: 1813–1816.

Mills AW (1958) On the minimum audible angle. J. Acoust. Soc. Am. 30: 237–246.

Molnar CE, Pfeiffer RR (1968) Interpretation of spontaneous spike discharge patterns of neurons in the cochlear nucleus. Proc. IEEE 56: 993–1004.

Neely ST, Kim DO (1986) A model for active elements in cochlear biomechanics. J. Acoust. Soc. Am. 79: 1472–1480.

Oertel D (1983) Synaptic response and electrical properties of cells in brain slices of the mouse anteroventral cochlear nucleus. J. Neurosci. 3: 2043–2053.

Oertel D (1999) The role of timing in the brain stem nuclei of vertebrates. Ann. Rev. Physiol. 61: 497–519.

Osen KK (1969) The intrinsic organization of the cochlear nuclei in the cat. Acta Otolaryngol. 67: 352–359.

Osen KK (1970) Course and terminations of the primary afferents in the cochlear nuclei of the cat: An experimental study. Arch. Ital. Biol. 108: 21–51.

Ostapoff EM, Morest DK (1991) Synaptic organization of globular bushy cells in the ventral cochlear nucleus of the cat: A quantitative study. J. Comp. Neurol. 314: 598–613.

Palmer AR, Russell IJ (1986) Phase-locking in the cochlear-nerve of the guinea-pig and its relation to the receptor potential of inner hair cells. Hearing Res. 24: 1–15.

Paolini AG, Clark GM (1998) Intracellular responses of the rat anteroventral cochlear nucleus to intracochlear electrical stimulation. Brain Res. Bull. 46: 317–327.

Paolini AG, Clark GM, Burkitt AN (1997) Intracellular responses of rat cochlear nucleus to sound and its role in temporal coding. NeuroReport 8: 3415–3422.

Paolini AG, Cotterill EL, Bairaktaris D, Clark GM (1998) Muscimol suppression of the dorsal cochlear nucleus modifies frequency tuning in rats. Brain Res. 785: 309–316.

Paolini AG, FitzGerald JV, Burkitt AN, Clark GM (2001) Temporal processing from the auditory nerve to the medial nucleus of the trapezoid body in the rat.

Papoulis A (1991) Probability, Random Variables, and Stochastic Processes (3rd ed.), McGraw-Hill, Singapore.

Perkel DH, Gerstein GL, Moore GP (1967) Neuronal spike trains and stochastic point processes. I. The single spike train. Biophys. J. 7: 391–418.

Pickles JO (1982) An Introduction to the Physiology of Hearing. Academic Press, London.

Plesser HE, Geisel T (1999) Markov analysis of stochastic resonance in a periodically driven integrate-fire neuron. Phys. Rev. E 59: 7008–7017.

Plesser HE, Tanaka S (1997) Stochastic resonance in a model neuron with reset. Phys. Lett. A 225: 228–234.

Rayleigh Lord (JW Strutt) (1876) On our perception of the direction of a source of sound. Nature Lond. 14: 32–33.

Retzius G (1884) Das Gehörorgan der Wirbeltiere. II. Das Gehörorgant der Reptilien, der Vogel und der Saugetiere. Samson and Wallin, Stockholm.

Rhode WS, Smith PH (1986) Encoding timing and intensity in the ventral cochlear nucleus of the cat. J. Neurophysiol. 56: 261–286.

Rose JE, Brugge JF, Anderson DJ, Hind JE (1967) Phase-locked response to low-frequency tones in single auditory nerve fibers of the squirrel monkey. J. Neurophysiol. 30: 769–793.

Rothman JS, Young ED (1996) Enhancement of neural synchronization in computational models of ventral cochlear nucleus bushy cells. Aud. Neurosci. 2: 47–62.

Rothman JS, Young ED, Manis PB (1993) Convergence of auditory nerve fibers onto bushy cells in the ventral cochlear nucleus: Implications of a computational model. J. Neurophysiol. 70: 2562–2583.

Rouiller EM, Cronin-Schreiber R, Fekete DM, Ryugo DK (1986) The central projections of intracellularly labeled auditory nerve fibers in cats: An analysis of terminal morphology. J. Comp. Neurol. 249: 261–278.

Ruggero MA, Rich NC (1987) Timing of spike initiation in cochlear afferents: Dependence on site of innervation. J. Neurophysiol. 58: 379–403.

Ruggero MA, Rich NC, Shivapuja BG, Temchin AN (1995) Auditory-nerve responses to low-frequency tones: Intensity dependence. Aud. Neurosci. 2: 159–186.

Ruggero MA, Robles L, Rich NC (1986) Cochlear microphonics and the initiation of spikes in the auditory nerve: Correlation of single-unit data with neural and receptor potentials recorded from the round window. J. Acoust. Soc. Am. 79: 1491–1498.

Ryugo DK, Fekete DM (1982) Morphology of primary axosomatic endings in the anteroventral cochlear nucleus of the cat: A study of the endbulbs of Held. J. Comp. Neurol. 210: 239–257.

Saint-Marie RL, Morest DK, Brandon CJ (1989) The form and distribution of GABAergic synapses on the principal cell types of the ventral cochlear nucleus of the cat. Hearing Res. 42: 97–112.

Salinas E, Sejnowski TJ (2000) Impact of correlated synaptic input on output firing rate and variability in simple neuronal models. J. Neurosci. 20: 6193–6209.

Sento S, Ryugo DK (1989) Endbulbs of Held and spherical bushy cells in cats: Morphological correlates with physiological properties. J. Comp. Neurol. 280: 553–562.

Smith PH, Rhode WS (1987) Characterization of HRP-labeled globular bushy cells in the cat anteroventral cochlear nucleus. J. Comp. Neurol. 266: 360–375.

Tasaki I (1954) Nerve impulses in individual nerve fibres of guinea pig. J. Neurophysiol. 17: 97–122.

Tolbert LP, Morest DK (1982) The neuronal architecture of the anteroventral cochlear nucleus of the cat in the region of the cochlear nerve root: Electron microscopy. Neurosci. 7: 3053–3068.

Tuckwell HC (1988) Introduction to Theoretical Neurobiology: Nonlinear and Stochastic Theories (Vol. 2). Cambridge University Press, Cambridge.

Tuckwell HC, Richter W (1978) Neuronal interspike time distributions and the estimation of neurophysiological and neuroanatomical paramaters. J. Theor. Biol. 71: 167–183.

von Békésy G (1960) Experiments in Hearing. EG Wever (ed. and trans.). McGraw-Hill, New York.

Walmsley B, Alvarez FJ, Fyffe REW (1998) Diversity of structure and function at mammalian central synapses. Trends Neurosci. 21: 81–88.

Webster DB, Popper AN, Fay RR (eds.) (1992) The Mammalian Auditory Pathway: Neuroanatomy. Springer, New York.

Young ED, Shofner WP, White JA, Robert JM, Voigt HF (1988) Response properties of cochlear nucleus neurons in relationship to physiological mechanisms. In: S Hassler, ed. Functions of the Auditory System. Wiley, New York. pp. 277–312.

Young ED, Rothman JS, Manis PB (1993) Regularity of discharge constrains models of ventral cochlear nucleus bushy cells. In: MA Merchan, J Juiz, eds. The Mammalian Cochlear Nuclei: Organization and Function. Plenum Press, New York. pp. 395–410.

Zhang S, Trussell LO (1994) A characterization of excitatory postsynaptic potentials in the avian nucleus magnocellularis. J. Neurophysiol. 72: 705–718.

Author/s:
Kuhlmann, L; Burkitt, AN; Paolini, A; Clark, GM

Title:
Summation of spatiotemporal input patterns in leaky integrate-and-fire neurons: Application to neurons in the cochlear nucleus receiving converging auditory nerve fiber input

Date:
2002-01-01

Citation:
Kuhlmann, L., Burkitt, A. N., Paolini, A. & Clark, G. M. (2002). Summation of spatiotemporal input patterns in leaky integrate-and-fire neurons: Application to neurons in the cochlear nucleus receiving converging auditory nerve fiber input. JOURNAL OF COMPUTATIONAL NEUROSCIENCE, 12 (1), pp.55-73. https://doi.org/10.1023/A:1014994113776.